



OPEN

SUBJECT AREAS:

GEOPHYSICS
SEISMOLOGY

Received

5 February 2014

Accepted

20 June 2014

Published

9 July 2014

Correspondence and
requests for materials
should be addressed to
F.R. (fabrizio.
romano@ingv.it)

Structural control on the Tohoku earthquake rupture process investigated by 3D FEM, tsunami and geodetic data

F. Romano¹, E. Trasatti¹, S. Lorito¹, C. Piromallo¹, A. Piatanesi¹, Y. Ito², D. Zhao³, K. Hirata⁴, P. Lanucara⁵ & M. Cocco¹

¹Istituto Nazionale di Geofisica e Vulcanologia, Rome, Italy, ²Disaster Prevention Research Institute, Kyoto University, Japan,

³Department of Geophysics, Tohoku University, Sendai, Japan, ⁴National Research Institute for Earth Science and Disaster Prevention, Ibaraki, Japan, ⁵CINECA, SuperComputing Applications and Innovation Department - SCAI, Rome, Italy.

The 2011 Tohoku earthquake ($M_w = 9.1$) highlighted previously unobserved features for megathrust events, such as the large slip in a relatively limited area and the shallow rupture propagation. We use a Finite Element Model (FEM), taking into account the 3D geometrical and structural complexities up to the trench zone, and perform a joint inversion of tsunami and geodetic data to retrieve the earthquake slip distribution. We obtain a close spatial correlation between the main deep slip patch and the local seismic velocity anomalies, and large shallow slip extending also to the North coherently with a seismically observed low-frequency radiation. These observations suggest that the friction controlled the rupture, initially confining the deeper rupture and then driving its propagation up to the trench, where it spreads laterally. These findings are relevant to earthquake and tsunami hazard assessment because they may help to detect regions likely prone to rupture along the megathrust, and to constrain the probability of high slip near the trench. Our estimate of ~ 40 m slip value around the JFAST (Japan Trench Fast Drilling Project) drilling zone contributes to constrain the dynamic shear stress and friction coefficient of the fault obtained by temperature measurements to ~ 0.68 MPa and ~ 0.10 , respectively.

On March 11th 2011 one of the largest earthquakes ever recorded occurred at the subduction interface between the Pacific and the Okhotsk plates and struck the Tohoku region in Japan (Fig. 1). This $M_w 9.1$ earthquake, located at 142.68°E 38.19°N , generated a tsunami that devastated the Japanese coasts, including towns and important infrastructures such as the Sendai airport and the Fukushima nuclear power plant causing more than 16,000 fatalities². The Tohoku earthquake is also the best observed ever megathrust event and consequently it has been investigated by modelling the unprecedented high-quality data set recorded by the Japanese dense seismological, geodetic and marine observational networks. The numerous studies published in recent literature are based on different kind of data and methodologies, including teleseismic³, strong motion⁴, geodetic^{5–7}, tsunami waveforms^{2,8}, and joint inversions^{9–11} which were performed to investigate the earthquake rupture process.

The resulting source models share two common features of the coseismic rupture, stimulating further investigations to explore the physical processes controlling the genesis and the impact of megathrust events. The first feature is that the overall Tohoku rupture area is mainly concentrated in a relatively small portion of the plate interface and the retrieved peak slip values range between 30 and 60 m. This long-wavelength feature is common to most of the slip models obtained using different kind of data. At the same time, differences in terms of maximum slip value or number of slip patches can be observed among models, due to the data resolution and fault parameterization^{4,7,10,12,13}. A rather small rupture area characterized by very large slip is quite unusual for great earthquakes such as the 2004, $M_w = 9.2$, Sumatra^{14,15} and the 2010, $M_w = 8.8$, Maule¹⁶ megathrust events. Some authors observed also a first order correlation between the coseismic slip patch and the positive seismic velocity anomaly at the subduction interface^{17–20}. The relatively concentrated Tohoku rupture area may be related to the lithosphere structure and the consequent heterogeneous pattern of pre-stress as well as to the fault frictional properties of the plate interface that could promote or inhibit the rupture propagation. The relative variations in shear-wave and bulk-sound speed detected in the coseismic slip area may reflect mechanical heterogeneities of the subduction interface, which may have acted as asperities allowing this event to build up large slip in the near-trench zone²¹.

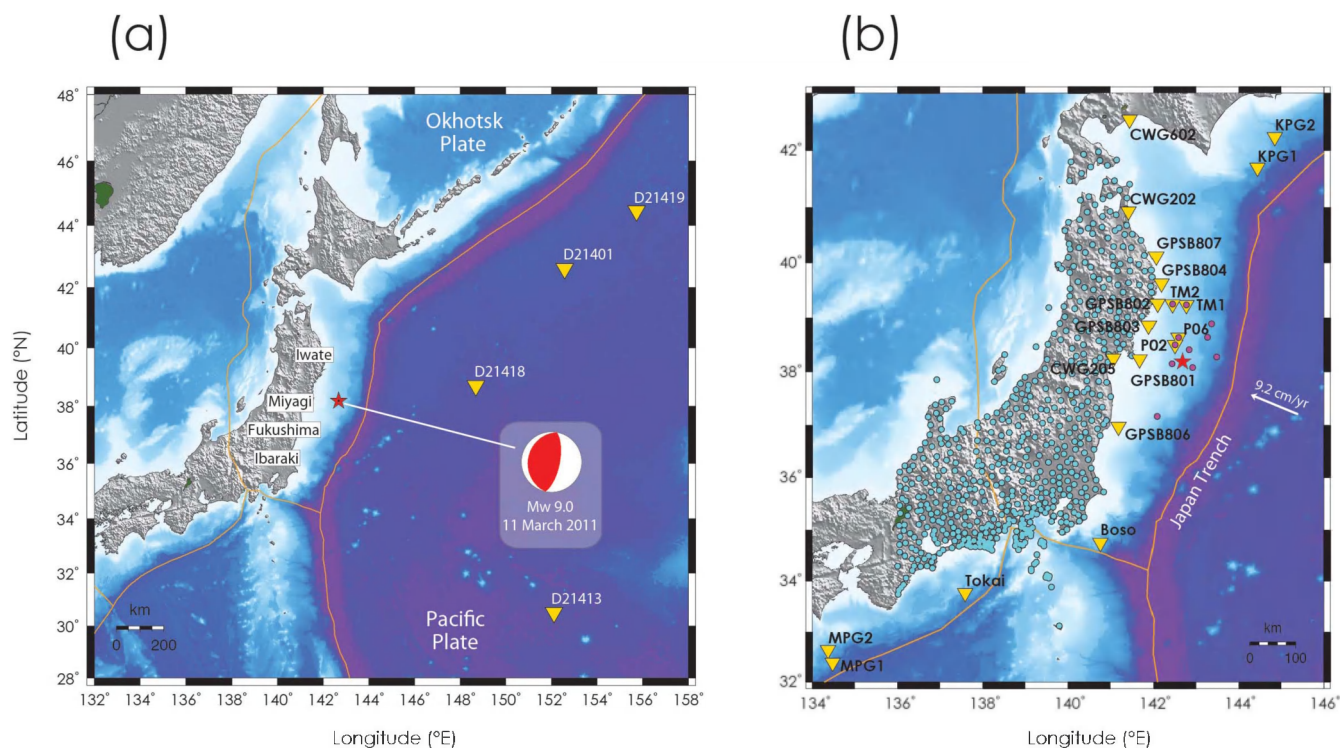


Figure 1 | Location Map. (a) Red star indicates the epicentre position. Red and white “beach ball” represents the focal mechanism of 2011 Tohoku earthquake. Yellow triangles indicate the DART stations used in the inversion; (b) Cyan circles indicate GPS stations onshore, magenta circles indicate the geodetic seafloor observation sites, yellow triangles indicate the bottom pressure sensors and GPS-buoys (Table S4 in Supplementary Information). White arrow indicates the approximate convergence direction of the Pacific plate (estimated velocity of 9.2 cm/yr). Maps are created using GMT (Generic Mapping Tools, <http://gmt.soest.hawaii.edu/>) software.

The second intriguing feature of the 2011 Tohoku earthquake is the shallow rupture propagation up to the trench^{2,4,10,13}. The large (>15 m) and shallow coseismic slip is at odds with the quite common view on the coseismic behaviour of the shallow portion of megathrusts, where aseismic slip, lack of strain accumulation and low coupling are expected to be dominant²². Recent results from the Japan Trench Fast Drilling Project (JFAST^{23–25}) pointed out the presence of smectite-rich weak clay, up-dip from the hypocentre in the very shallow portion of the subduction plate boundary. Thus, this distinctive feature of the Tohoku earthquake might have been controlled by very low friction²⁶ on a relatively thin fault zone rich of clay sediments^{24,25,27}.

Both these features, contributing to confine a vertical seafloor displacement larger than 10 m in a relatively small area^{2,10}, may have increased the tsunamigenic potential of the 2011 earthquake, generating tsunami waves higher than 10 m and runups larger than 30 m along the Iwate prefecture coasts²⁸.

Accounting for detailed information on the geometry and structure of the subducting plate is necessary in order to reduce the epistemic uncertainties related to the modelling, to get a robust image of the coseismic slip distribution, to further constrain its spatial extension with respect to previous studies, and to focus on the shallow near-trench portion of the megathrust. We achieve this by carrying out, for the first time to our knowledge, a joint inversion of tsunami and both inland and seafloor geodetic data, constraining the slip distribution by means of a 3D Finite Element Model (FEM) of the subduction zone. We characterize each single element of the FEM grid by the 3D elastic structure inferred from seismic tomography²⁹, whereas the shallow near-trench portion of the megathrust, rich of sediments, is modelled by assuming a much more compliant material with respect to the surrounding medium (see section Methods). Our modelling approach enables to account for the effects of the elastic

contrasts both within the crust and between the crust and the mantle and, furthermore, for mimicking the contrast between the crust and the sediments at the trench (i.e. clay-rich sediments), which may play a key role in controlling the coseismic slip distribution.

Aim of this work is to image the slip distribution adopting a more realistic representation of the Green’s functions through the 3D FEM model. In particular, we discuss whether and how the rupture extent and its propagation near the trench have been controlled by the regional and fault-zone structural heterogeneities. We also relate the shallow slip propagation to the recent JFAST results, drawing some possible relationships with the observed seismic radiation.

Results

The 3D geometry of the FEM (cf. section Methods for details) is built taking into account the main features of the subduction zone including the Tohoku region, such as the slab geometry and the topography/bathymetry. A FEM mesh of about 280,000 8-nodes brick elements is then created (Fig. 2). The 3D elastic structure of each element is constrained by the 3D P-wave and S-wave velocities (V_p and V_s , respectively) of a regional tomographic model²⁹; the resulting crust, slab and mantle are highly heterogeneous, with rigidity values ranging from ~20 GPa in the crust, to ~50–60 GPa in the slab. The elastic structure of the shallow part of the megathrust (i.e. the prism above the subduction fault) is characterized by independent data as imaged by seismic reflection surveys^{30,31}. The prism volume is limited by the trench to the East and by a steep listric plane to the West³⁰ and is considered as made of unconsolidated clay-rich sediments and volcanic materials, for which we assume uniform elastic constants (rigidity = 5 GPa and Poisson’s ratio = 0.33). The chosen elastic values are compatible with those attributable to weak-clay (smectite) observed by the JFAST drilling project^{23–25}.

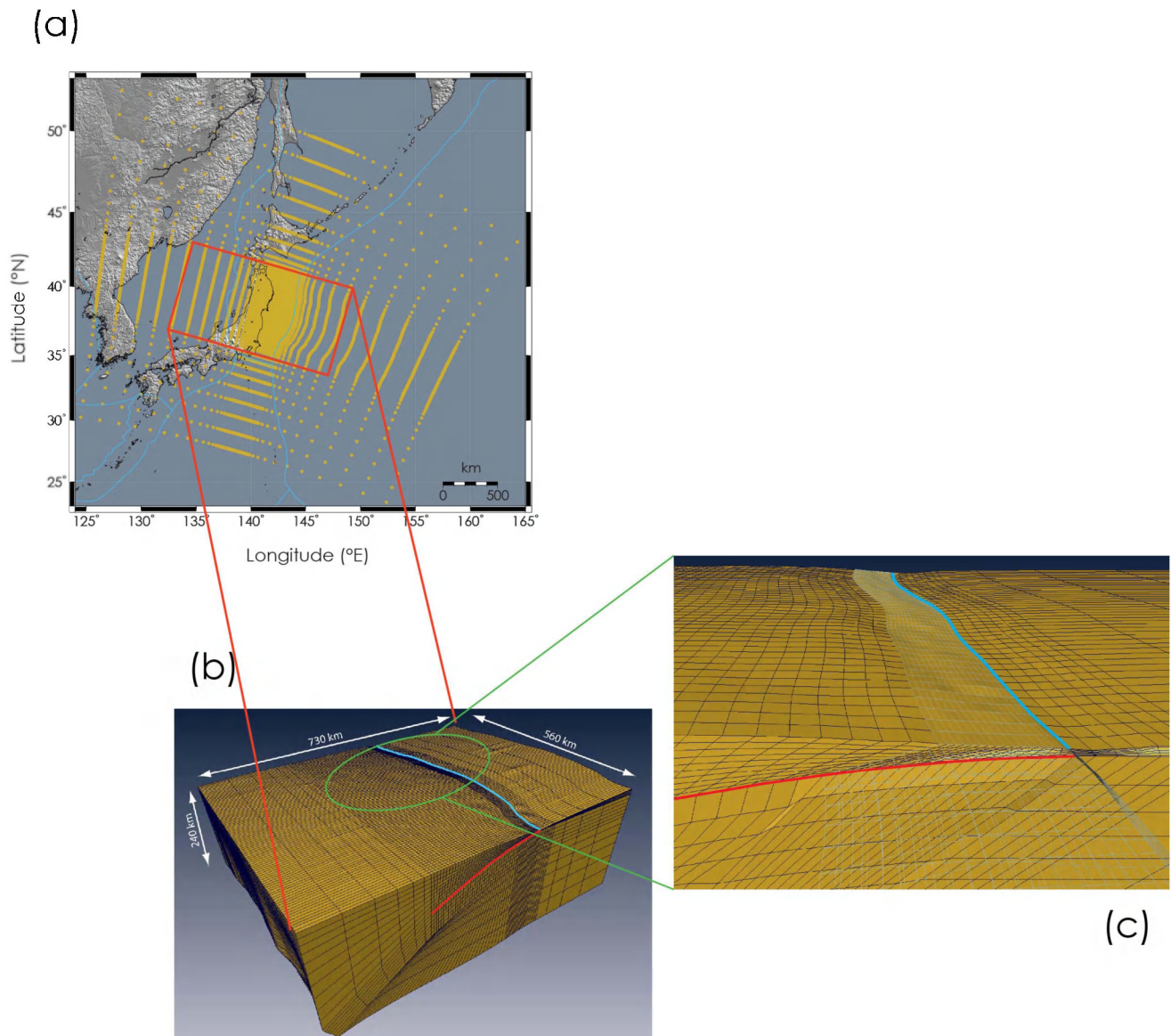


Figure 2 | FEM model. (a) Total domain of the 3D FEM model ($\sim 2900 \times 2500 \text{ km}^2$). Yellow dots represent the free surface grid nodes. (b) Central part of the 3D FEM model, including the active fault, viewed from SW. The light blue line is the trench and the red line is the section of the active fault. (c) The inset shows a zoom of the interface between trench and the uppermost part of the fault. The shaded element edges lines on the top identify the prism extent. Details about the elastic layering of the model can be found in the Supplementary Information, Figure S1. Panel (a) is created using GMT software, panels (b,c) using AMIRA (<http://www.vsg3d.com/amira/overview>, Date of access: 11/06/2011) software.

The FEM model is then used to compute a set of Green's Functions which are combined with a robust joint inversion scheme adopted in several previous papers to retrieve the slip distribution^{10,14,15,32,33}. The inverse problem is solved by using the method of Green's functions superposition and the Heat Bath algorithm, a particular implementation of the Simulated Annealing technique³⁴. The slip distribution is obtained through a global search technique³⁵. Since the solution of this inverse problem is intrinsically non-unique³⁶, and to account for possible modelling uncertainties, we compute and show the average slip model that we consider more representative than the best fitting solution¹⁶. The average slip model is calculated as a weighted mean of a subset of the explored models. We assess the dispersion of the model parameters around their average values by performing an a-posteriori analysis of the explored models ensemble so that the error associated to each parameter is its weighted standard deviation^{10,14,15,32,33}. In this analysis the coefficient of variation (i.e. the standard deviation divided by the average slip value) is also

computed for each subfault parameter (further details in Methods section).

The 2011 Tohoku earthquake slip distribution. The slip distribution of the 2011 Tohoku earthquake (Figure 3a) extends mainly along strike from $\sim 36.5^\circ\text{N}$ to $\sim 39.5^\circ\text{N}$ and up-dip from the hypocentre in the SE direction (from $\sim 142^\circ\text{E}$ to $\sim 144^\circ\text{E}$). The portion of megathrust with slip values greater than $\sim 10 \text{ m}$ (i.e. $\sim 20\%$ of the maximum peak of slip) corresponds to an area of about $350 \times 200 \text{ km}^2$. Amplitudes ranging between 25 m and 30 m characterize the slip distribution in the earthquake nucleation zone. Slip amplitudes increase moving away from the hypocentre towards the trench; slip direction is consistent with both the relative convergence of the Pacific and the Okhotsk plates and the centroid moment tensor solution (GCMT). Rake angle averaged over the whole slipping area is $\sim 88^\circ$. The rupture reaches the shallow and less locked part of the megathrust with slip values

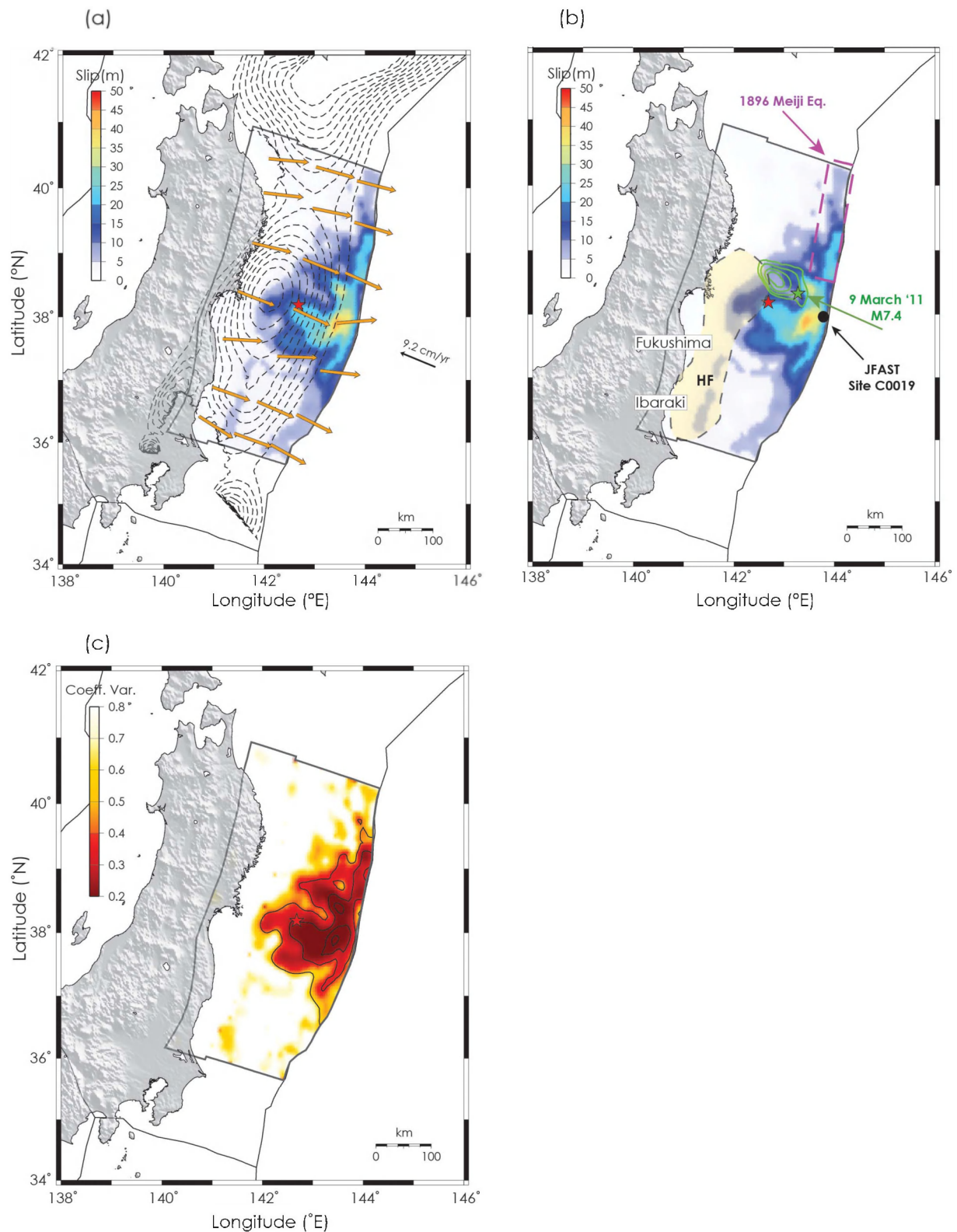


Figure 3 | Slip distribution. Slip distribution for the 2011 Tohoku-oki earthquake obtained from the joint inversion of tsunami and geodetic data. (a) Orange arrows represent the slip direction (rake, Table S3 in Supplementary Information). Thin dashed black contours above the fault plane indicate the interseismic coupling⁴⁸ (from 10% to 100%, at 10% intervals) along the megathrust. Black arrow indicates the approximate convergence direction of the Pacific plate (estimated velocity of 9.2 cm/yr). Red star as of Figure 1. (b) Green contour lines (intervals are at 0.25, 0.50, 1.00, and 1.50 m) and green star indicate the slip distribution and the epicenter position of the foreshock⁴⁵ occurred on 9 March 2011, respectively; magenta dashed rectangle represents approximately the rupture area of the 1896 Meiji-Sanriku earthquake²; yellow coloured region approximately indicates the zone of coseismic high frequency radiation; black dot indicates the JFAST ocean drilling site C0019²³; (c) coefficients of variation associated to the average slip model of the 2011 Tohoku-oki earthquake resulting from the joint inversion. Black contour lines (10meters interval) indicate the slip distribution of Tohoku earthquake. Maps are created using GMT software.



greater than 30 m, up to ~ 45 m around $\sim 143.5^\circ\text{E}$, 38°N . The inferred slip distribution shown in Figure 3b displays a narrow patch of slip located to the NE (from $\sim 38.5^\circ\text{N}$ to $\sim 39.5^\circ\text{N}$) in the shallow part of the subduction interface roughly corresponding to the area where the 1896 Meiji-Sanriku earthquake occurred³⁷. In addition, at around 35 km depth a relatively low slip feature extends from the hypocentre zone to the latitudes of Fukushima and Ibaraki prefectures. This feature, generally imaged by using strong-motion and seismic data^{4,13}, approximately corresponds to a source of high frequency radiation detected by means of back-projection analysis¹² and amplitude source location method³⁸. Even though our inverted distribution represents a long-wavelength image of the coseismic slip pattern, the complex model adopted and the inversion technique allow sensing this peculiarity of the Tohoku earthquake even using only tsunami and geodetic data. We recognize, however, that the pattern of the variation coefficient (Figure 3c) indicates that the slip distribution is particularly well resolved (variation coefficient lower than ~ 0.4) in the portion of megathrust with slip values greater than 10 m.

The estimated total seismic moment, computed by taking into account the elastic parameters used into the FEM model (see Methods section) is $M_0 = 5.72 \times 10^{22}$ Nm, corresponding to a magnitude $M_w = 9.1$.

The inferred slip model (Fig. 3a) yields a general good fit to tsunami (RMS = 0.50 m) and geodetic (RMS = 0.38 m, 0.19 m, and 0.14 m for East-West, North-South, and vertical components, respectively) data (Fig. 4). It is noteworthy that the tsunami signals measured by the GPS-buoys off Iwate (G802, G804, G807) and by the bottom pressure sensors located very close to the source are extremely well reproduced, in particular their short-period wavelengths. This feature is probably tied up to the narrow patch of slip located in the shallow part of the megathrust from $\sim 38.5^\circ\text{N}$ to $\sim 39.5^\circ\text{N}$. However, a slight phase shifting is observed at few tsunami stations (e.g. G801) and it may be due to our assumption of a simplified circular rupture front (propagating from the hypocenter with a velocity of $1 \text{ km/s}^{39,40}$) while the actual rupture history of Tohoku event^{4,41} is likely more complex.

We also notice, as already observed in previous studies^{2,11}, that the tsunami amplitude is amplified by the contribution of the horizontal seafloor deformation near the trench axis (due to the presence of steep bathymetric slopes⁴², further details in section Methods). This effect is particularly evident for the stations located near or above the source region (TM1, TM2, P02, P06, G802, G804, G807) where the wave amplitudes are smaller by ~ 20 – 40% if the horizontal deformation contribution is not included (Supplementary Figure S3).

The present slip model confirms at the first order the rupture pattern retrieved in our previous study¹⁰ as well as in other works^{2,4,5,7,9,11–13,43,44}, i.e. the large slip in a relatively concentrated rupture area and the shallow rupture propagation. In particular, a shallow patch of slip in the northern portion of the megathrust is clearly distinguishable, a feature also observed using seismic data^{4,12,13,44} and that will be discussed in a later section. In addition, the present slip model highlights a new interesting feature, thanks to the employment here of an enlarged geodetic and tsunami data set (particularly above the source, e.g. P02 and P06 sensors), and of a FEM model honouring the structural heterogeneities. Indeed, we observe a relative minimum of slip (< 10 m) close to 38.5°N , 143°E (Figure 3b) that overlaps with the main rupture area of the foreshock ($M_w = 7.4$) occurred on 9 March 2011⁴⁵. This distinctive feature may be attributed to a low pre-stress level due to the foreshock occurrence; actually, a negative stress change has been estimated in the portion of megathrust slipped during the foreshock⁴⁵.

Rupture extent, seismic velocity anomalies and frictional properties. The mechanism of generation, propagation and arrest of an earthquake may depend on different factors such as 3D

structural heterogeneities of the medium, the frictional properties of the source zone, and the stress load. The seismic velocity anomalies at the fault-scale could represent a reasonable proxy to describe the variability of the above-mentioned features^{18,21,46}. Moreover, some authors¹⁸ observed that in the rupture area of the Tohoku earthquake the seismic velocity anomalies are correlated with the slip distribution obtained by inverting only inland GPS data⁴⁷. Here, we compare our slip distribution with the high-resolution tomographic model at the subduction interface²⁹ in order to better understand how much the Tohoku rupture has been controlled by structural heterogeneities (i.e. seismic velocity anomalies) at the fault-scale.

Three distinct zones, remarkably evident for Vp anomalies distribution, are present along the seismogenic portion of the slab interface, in a well-resolved region of the tomographic model²⁹. We observe in Figure 5a a Positive Velocity Anomaly zone (hereinafter PVA) centred at $\sim 38^\circ\text{N}$, $\sim 142.5^\circ\text{E}$, whereas two Negative Velocity Anomaly zones (hereinafter NVA) are located just to the North and to the South of the PVA (centred at $\sim 39.5^\circ\text{N}$, $\sim 143^\circ\text{E}$ and $\sim 37^\circ\text{N}$, $\sim 142.5^\circ\text{E}$, respectively). A very strong spatial correlation is observed between the slip distribution (slip > 10 m) and the PVA present in the Vp model; the rupture area almost completely overlaps the PVA zone ($> 70\%$ of the slipping area) and borders the NVA zones. Such a correlation holds for the Vs anomalies as well (Fig. 5b). This close correspondence suggests that the Tohoku rupture might have been efficiently controlled by the observed velocity anomalies, perhaps associated to the variation of the frictional properties of the Tohoku megathrust zone.

Comparison with the map of interseismic locking⁴⁸ at seismogenic depth ($> \sim 20$ km, where the coupling estimation is well resolved) shows that the coupling degree is very high ($> \sim 80\%$) in the PVA zone (Figs. 5a,c), while it decreases ($< \sim 50\%$) moving toward both the NVA zones. In principle, zones with relatively low coupling are assumed to be creeping and having a velocity strengthening behaviour, while locked zones, where the earthquakes generally occur, are assumed to have a velocity weakening behaviour^{49–51}. Hence, we infer that the NVA zones, characterized by relatively low coupling, and the PVA zone, that is the most locked, exhibit a velocity strengthening and velocity weakening behaviour, respectively. This interpretation is supported by the observation that past large interplate earthquakes ($M > 7$ occurred since 1900 along the Tohoku region) are distributed preferentially inside the areas characterized by PVA¹⁸ as shown in Figures 5a,b.

In summary, the absence of large past earthquakes, the low coupling, and the relatively confined spatial extent of the Tohoku earthquake rupture area (mainly restricted to the PVA region) considered together suggest a possibility that the NVA may have acted as velocity strengthening zones. This hypothesis accounts for the unexpected and very high slip in a relatively small area, conflicting with expected values from empirical earthquake scaling laws⁵². The fact that a relatively small percentage of the rupture area ($< 30\%$) lies within the NVA zones is not at odds with this interpretation. Such a feature is not unusual for great earthquakes such as the one occurred in Tohoku. Indeed, a recent study has demonstrated that under specific conditions great earthquakes ruptures might propagate, even partially as in the present case, through velocity strengthening zones⁵¹.

A further analysis of the seismic velocity anomalies provides insights about the possible fluids content along the subduction interface nearby the Tohoku hypocenter. Actually, the earthquake nucleation may be also related to the distribution of fluids around the plate boundary⁵³. The earthquake nucleated in a strongly coupled zone that is characterized by both PVA and Positive Vp/Vs Ratio Anomaly (PVRA from here on, Fig. 5d). The PVRA may indicate presence of fluids in brittle rocks⁵⁴. As a consequence, excess pore pressure might have decreased the strength on the fault plane and caused the main shock occurrence.

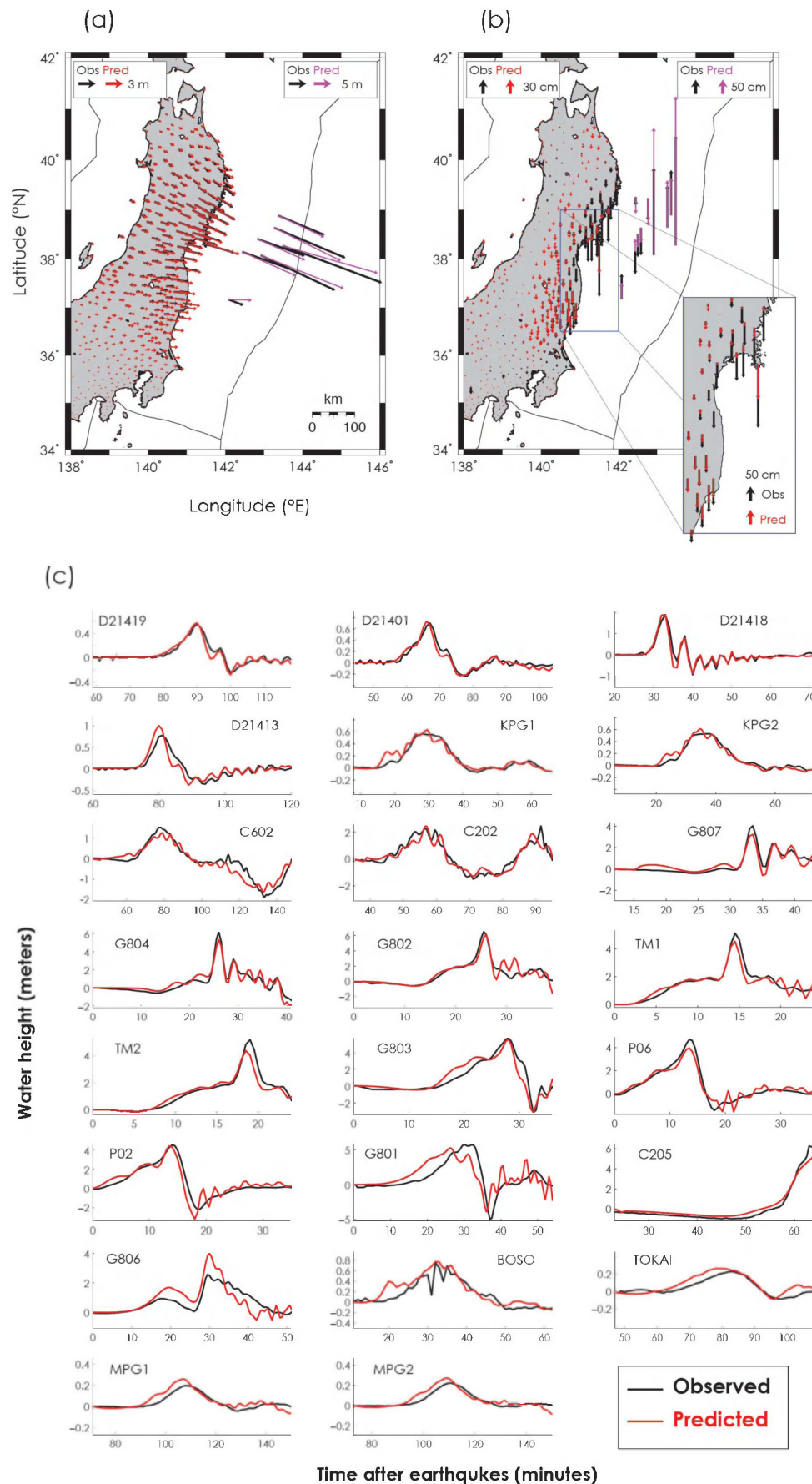


Figure 4 | Comparison between observed and predicted data sets. Comparison between observed (black) and predicted (a) horizontal and (b) vertical displacements at GPS (red) and geodetic seafloor observation sites (magenta). (c) Comparison between the observed (black) and predicted (red) tsunami waveforms. Panels (a,b) are created using GMT software; panel (c) using MATLAB (<http://www.mathworks.it/products/matlab/>, Date of access: 11/06/2011).

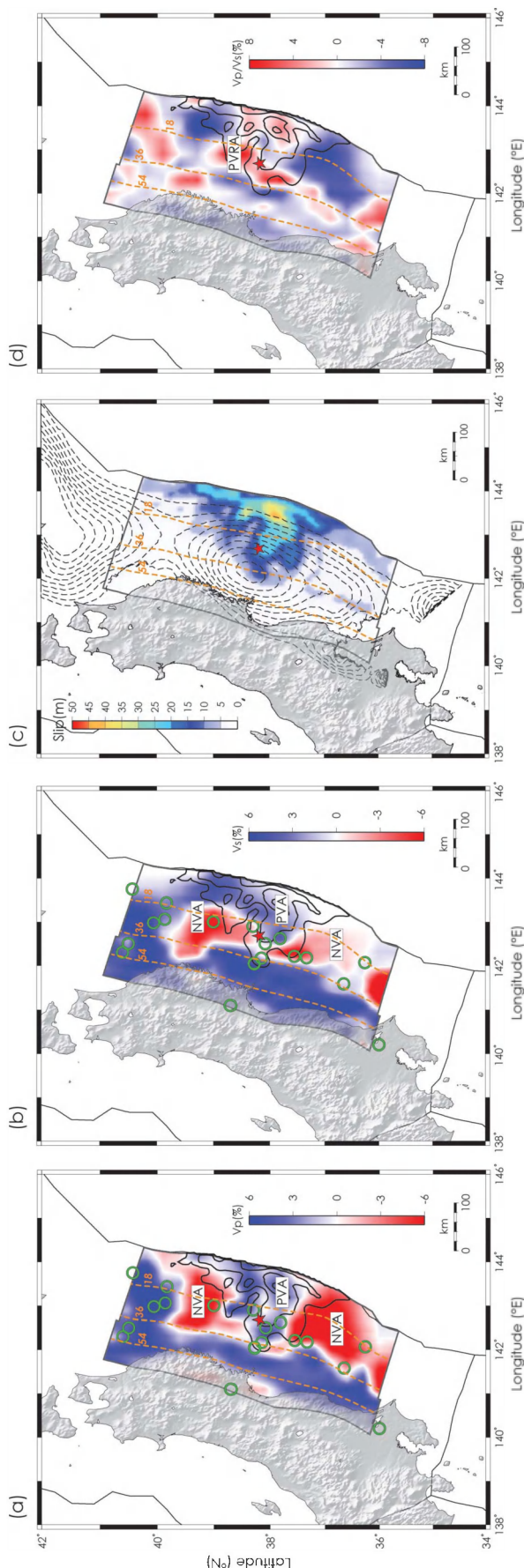


Figure 5 | Comparison between Slip and Velocity anomaly distributions. (a) V_p and (b) V_s anomaly distributions²⁹ on the subducting plate

interface. Black contour lines (10 m interval) indicate the slip distribution of Tohoku earthquake. Open green circles indicate the large ($M > 7$) earthquakes occurred in the Tohoku earthquake region since 1900. Orange dashed contour lines (18 km interval) indicate the depth of plate interface. Red star as of Figure 1. (c) Slip distribution for the 2011 Tohoku-oki earthquake. Red star and thin dashed black contours above the fault plane as of Figure 3a; (d) V_p/V_s ratio anomaly distribution on the subducting plate interface. Black contour lines (10 m interval) indicate the slip distribution of Tohoku earthquake. Red star as of Figure 1. Maps are created using GMT software.

In the light of all of the above, we suggest that the velocity strengthening zones may have initially acted as barriers to rupture propagation, laterally confining it to the relatively small area around the earthquake nucleation point. Subsequently, due to the coseismic weakening and the local very heterogeneous frictional conditions^{24,25,27}, the rupture has been driven towards the trench where it further propagated and spread laterally along strike in the low friction shallow part of the subduction zone, as shown by the slip model (Fig. 3a). The shallow slip propagation will be more thoroughly analysed in the next section.

Shallow slip propagation. The slip distribution retrieved in the present study and most of the published source models^{2,4,9,10,13,55} highlight large slip values (>15 m) in the shallower part of the subducting interface (depth $< \sim 15$ km) from $\sim 37^\circ\text{N}$ to $\sim 39.5^\circ\text{N}$, with peak values greater than ~ 35 m nearby 143.5°E , 38°N . Since the shallowest part of megathrusts is commonly thought to be characterized by a rate strengthening behaviour²² and dominated by aseismic slip, lack of strain accumulation and low coupling, the large shallow slip occurred during the Tohoku earthquake came as a surprise.

Numerical modelling of the dynamic rupture⁵⁶ and laboratory experiments on clays²⁷ hypothesized dynamic weakening of the fault at high slip rate as the possible reason for the large slip near the trench. This hypothesis is corroborated by the results of JFAST project^{23–25} that conducted a drilling survey near the Japan trench (site C0019, Fig. 3b). In particular, dynamic shear stress and friction coefficient were determined by the temperature measurements at the plate boundary²⁴ and by laboratory friction experiments²⁵ under conditions of both low permeability and high slip velocity. The JFAST results as a whole indicate low shear stress, low friction on the fault, and low permeability conditions of smectite-rich clays within the décollement, thus supporting the coseismic weakening of the fault. The estimation of the friction coefficient from temperature has been obtained by assigning a value for slip, which is one of the greatest uncertainties in the estimates of shear stress and friction. A fault slip of 50 m is assumed²⁴ at the site C0019, in agreement with some previously published slip models. In this area our model indicates instead a lower slip value of ~ 40 m (Fig. 3a), which would imply average shear stress and friction coefficient of ~ 0.68 MPa and ~ 0.10 respectively (Patrick Fulton, personal communication). These values are slightly higher with respect to estimates using 50 m of slip but still in the range of values obtained experimentally for slip greater than ~ 35 m under different permeability conditions²⁵.

The slip distribution found in the present study features a rupture pattern further extending to the northern portion of the Tohoku region, in a narrow and shallow stripe from $\sim 38.5^\circ\text{N}$ to $\sim 39.5^\circ\text{N}$, with slip values up to 26 m (Fig. 3b). The northern patch of slip roughly overlaps the estimated rupture area of the $M_w = 8.0\text{--}8.2$ ⁵⁷ 1896 Meiji-Sanriku earthquake^{2,37}. The maximum tsunami runup heights caused by the Tohoku event along the Iwate prefecture coasts and those caused by the 1896 Meiji-Sanriku tsunami earthquake⁵⁸ are comparable²⁸. Some authors^{2,8} examined possible similarities between the causative source of this shallow past tsunamigenic event



and the shallow part of the Tohoku rupture. The 1896 event has been characterized by a very weak high-frequency seismic radiation and a long rupture duration⁵⁸, and it has been classified as a tsunami earthquake. A slow component in the source of the 2011 Tohoku event is not detected by using long-period spheroidal modes of the Earth⁵⁹, but this could be likely due to the lack of sufficient resolution at a local scale. Contrarily, different images of the radiated energy obtained in recent studies about the Tohoku earthquake are compatible with the hypothesis of slow rupture for the northern patch of slip. Indeed, in this zone a weak high-frequency seismic radiation feature has been observed⁴³, whereas a strong low-frequency seismic radiation contribution has been identified to the North of $\sim 38.5^\circ\text{N}$ ¹². The simultaneous presence of strong low-frequency and weak high-frequency radiation in the area to the north of $\sim 38.5^\circ\text{N}$ may indicate a relatively slow rupture⁶⁰. This hypothesis is also consistent with the low slip rate in the same region⁴⁴. Therefore, a shallow slow rupture with associated very large slip, in principle, is compatible with a tsunami earthquake mechanism. Nevertheless, some authors⁶ claim that a submarine landslide is required in place of this patch of slip. Their slip model, derived only by geodetic data inversion, which clearly may have only a local resolving power on the slip distribution, indeed fails in predicting the tsunami signals at GPS-buoys off Iwate prefecture (i.e. GPS-buoys 802, 804, and 807) and therefore they need to invoke an additional tsunami generation mechanism to reproduce these data. The impulsive and short-period tsunami signal measured by the above-mentioned GPS-buoys and both TM1 and TM2 sensors are probably due to the short wavelength offshore seafloor deformation generated by the large and shallow slip in the Tohoku region². Therefore, we observe that the tsunami signals observed at GPS-buoys off Iwate (Figure 4c) are in principle fully compatible with a narrow and shallow patch of slip as the one in Figure 3, derived by our joint inversion.

In conclusion, the coseismic slip is overall coherent with the observed seismic radiation and it is sufficient to reproduce the short-period tsunami signals without invoking additional tsunami sources. Even if this reasoning does not rule out the hypothesis of a landslide, it shows at least that such a contribution to the tsunami source is not strictly necessary to explain the observed data, as the differences with synthetic data are likely to be well within epistemic uncertainties. In order to be confirmed, the hypothesis of such a huge mass movement would need additional supporting evidence, e.g. a dedicated bathymetric survey.

Discussion

We derived the slip distribution of Tohoku earthquake by performing a joint inversion of tsunami and geodetic data combined with 3D FEM technique. This novel approach based on high-quality data, and the modelling of geometrical and structural heterogeneities of the source zone permitted us to obtain an accurate image of the slip, particularly near the Japan trench. Our slip distribution is characterized by very large slip values (up to ~ 45 m) in a relatively concentrated rupture area that extends up to the trench with slip values greater than 30 m. The features of the retrieved slip model are compatible with the sources of high- and low-frequency seismic radiation of the Tohoku earthquake identified by back-projection¹² and source location methods³⁸.

Moreover, we investigated whether the slip distribution might have been controlled by structural or frictional heterogeneities at the fault-scale. The slip image shows an unprecedented spatial correlation with the positive seismic velocity anomalies, with the rupture area overlapping by more than 70% the positive anomaly zone and bordering the negative anomalies. We suggest that the negative anomaly zones have acted as velocity strengthening barriers for the rupture propagation. This hypothesis accounts for the unusual shallow and very large slip in a relatively small area, which consequently may have increased the tsunamigenic potential of the earthquake.

Finally, we examined the shallow rupture propagation of the earthquake. The large and shallow slip values we found in the central part of the fault are compatible with the results of JFAST drilling survey^{23–25}, even if our slip value (~ 40 m) indicates slightly higher dynamic shear stress and friction coefficient. Consistently with the results of strong-motion and seismic inversion, we also found a shallow slip patch along the fault portion roughly corresponding to the rupture area of the 1896 Meiji-Sanriku tsunami earthquake. This patch of slip is reconcilable with some images retrieved by back-projection technique corroborating the hypothesis of a slow rupture component and, implicitly, a tsunami earthquake mechanism. Our results also show that a seismic source is sufficient to explain the Tohoku earthquake rupture process and to reproduce the ensuing short-period tsunami signals without invoking additional tsunami sources.

In conclusion, our findings encourage further studies to verify the correlation between the velocity anomalies and the megathrust ruptures, as well as the trench structure and material properties, in other subduction zones. This kind of studies can be of utmost importance for long-term earthquake hazard assessments, because they may help to detect regions likely prone to rupture along the megathrust, and even more for tsunami hazard assessments, if they can help constraining the probability of high slip in the trench region.

Methods

Tsunami data. Tsunami waves generated by the Tohoku earthquake have been recorded by many instruments positioned near the Japanese coasts (GPS-buoys, coastal wave gauges, bottom pressure sensors), above the source area (bottom pressure sensors) and in the open ocean (DART buoys).

The original signals include the tide and in some cases the surface waves generated by the earthquake. Tides are removed by using a procedure based on robust LOWESS. Further details about tsunami data are in Supplementary Information.

Geodetic data. The stations of the GPS Earth Observation Network (GEONET) of Japan have recorded the coseismic deformations associated with the Tohoku earthquake. GPS data used in this study are distributed mainly along the Honshu Island and the southernmost part of the Hokkaido Island where a distinct coseismic deformation has been measured. The Geospatial Information Authority (GSI) of Japan has provided all original data and their processing is described in a previous work published by the same authors¹⁰.

The large coseismic deformation has been estimated also on the seafloor by some geodetic observatories operated by Japan Coast Guard⁶¹ and by Tohoku University^{62,63} by a GPS/acoustic combination technique. The coseismic seafloor deformations have been measured as difference between the positions observed before and after the 2011 event exploiting the acoustic transponder technology. Furthermore, additional vertical seafloor geodetic measurements have been obtained by some ocean bottom pressure gauges positioned above the seismic source^{7,62}.

FEM. The free surface of the FEM is determined by means of a 250 m spatial resolution topographic/bathymetric digital model provided by the Hydrographic and Oceanographic Department (HOD) of the Japan Coast Guard. The data cover the whole top area of the FEM domain, about $2900\text{ km} \times 2500\text{ km}$ (from 125°E to 163°E and from 15°N to 52°N , Fig. 2). The geometry of the megathrust is constrained by the slab model for subduction zones (Slab1.0⁶⁴), available at <http://earthquake.usgs.gov/research/data/slab/#models> (Date of access: 11/06/2011). The obtained interface extends for 550 km from 35.4°N to 40.4°N , latitudes of intersection with the trench, and it follows the curvature depicted by the slab down to about 70 km depth, which is the supposed fault's bottom (Fig. 2). Along the Japan trench the topographic/bathymetric and the slab surfaces have a variable vertical distance ranging between 1 km and 3.5 km. The discrepancy at the trench is due to the different origin of the two 3D digital surface models and to the degraded slab surface resolution at the trench. The slab, whose thickness is 45–70 km, penetrates down to 600 km depth with a dip angle of 45° ^{17,29}.

The spatial resolution of the grid is 3 km close to the trench and 6 km in the remaining fault, while the element dimension increases toward the lateral and bottom edges of the computational domain. The fault plane is subdivided into patches of variable size: $24\text{ km} \times 14\text{ km}$ (length \times width) close to the trench (up to $\sim 15\text{ km}$ depth), $24\text{ km} \times 24\text{ km}$ in the central part up to $\sim 40\text{ km}$ depth (corresponding to more than 2/3 of the fault surface) and $35\text{ km} \times 35\text{ km}$ in the deeper part. Null displacements are assigned to the bottom boundary of the numerical domain. The 3D elastic structure is constrained by the 3D V_p and V_s local earthquake tomography²⁹, where the whole Honshu arc (from the Japan trench to the backarc in the Japan Sea) is mapped by inverting a high-quality data set of P- and S-wave arrivals, both from earthquakes prior to the Tohoku event and occurring under the land area and seismic events beneath the Pacific Ocean and Japan Sea. The suboceanic events help to constrain the 3D velocity model under the Pacific Ocean more reliably. The absolute seismic velocities are transformed into elastic parameters using



$$V_p = \sqrt{\frac{\lambda + 2\mu}{\rho}} \quad (1)$$

and

$$V_s = \sqrt{\frac{\mu}{\rho}} \quad (2)$$

where (λ, μ) are the Lamé's constants (medium considered isotropic) and ρ is the density. The density is assigned to each layer defined^{65,66} in the FEM model (Supplementary Information, Fig. S1, Table S1). Note that each element of the grid is characterized independently based on the 3D seismic velocities⁶⁷, without layering approximation that is referred to the density only.

The 10 km vertical resolution of the tomographic model is too coarse to allow constraining the seismic velocities at shallow depths close to the trench, where more compliant material with respect to the surroundings is likely present²⁹. Therefore we use independent data from seismic reflection surveys^{30,31} to properly describe the volume above the fault and across the trench, considering the shallow prism volume as made of sedimentary (such as clay-rich sediments) and volcanic materials, for which we assume uniform elastic constants^{30,31}.

Geodetic Green's functions. Green's functions at GPS stations and seafloor observation points are generated by means of the FEM. The active fault is subdivided into 398 subfaults (Supplementary Information, Fig. S2, Table S2) composed of pairs of coincident nodes. Each Green's function is computed by imposing kinematic constraints at the nodes of the FEM grid pertinent to the considered subfault. Since each subfault is made of several dislocating nodes, the slip may reach very shallow depths, close to the trench (~1 km). The coincident nodes of the active subfault dislocate a relative fixed amount Δu along the rake direction, while moving together in the perpendicular directions. The remaining pairs of coincident fault nodes are constrained to move together of the same amount (i.e., no dislocation among coincident nodes). The displacement is not distributed as $-\Delta u/2$ and $+\Delta u/2$ at both sides of the subfault, but the amount at each side depends on the subfault dip, the distance from the free surface, and the local elastic parameters contrast. FEM computations are carried out using the commercial software Abaqus, version 6.9⁶⁸.

Tsunami Green's functions. The initial condition for tsunami propagation is generally represented by the water displacement associated to the vertical seafloor deformation. However, in the regions of steep bathymetric slopes the contribution of the seafloor coseismic horizontal deformation may be not negligible with respect to the vertical one^{11,42}. Thus, the tsunami initial condition is computed as

$$u = u_x + u_y \frac{\partial H}{\partial x} + u_z \frac{\partial H}{\partial y} \quad (3)$$

where u_x , u_y , and u_z are the components of the coseismic displacement in the east, north and vertical direction respectively, H is the bathymetry depth (positive downward) and u is the final tsunami initial condition. The components u_x , u_y , and u_z are numerically computed by Abaqus as well. The tsunami Green's functions for each subfault then are modelled by means of NEOWAVE^{69,70}, a nonlinear dispersive wave model for tsunami propagation. The code numerically solves the nonlinear shallow water equations by using a semi-implicit finite difference technique on a staggered grid. In order to take into account the weakly dispersive behaviour of tsunami propagation, in NEOWAVE the equations include a non-hydrostatic pressure term and a vertical momentum equation. For tsunami modelling we use a computational domain with a spatial resolution of 1 arc-min, and the bathymetric digital model provided by HOD opportunely resampled.

Inversion. We follow a joint inversion scheme whose reliability has been already implemented in several previous papers^{10,14,15,32,33,71} to retrieve the coseismic slip distribution of the 2011 Tohoku-oki earthquake (further details in Supplementary Information). Two different cost functions for tsunami and geodetic data are used. For tsunami data we use a function that results to be sensitive in matching both phases and amplitudes of the time series⁷². Instead, a standard L2 norm is used for the geodetic data set.

Previous studies on the Tohoku earthquake highlighted the importance of having tsunami and geodetic data just above the source in order to better constrain the earthquake slip distribution^{10,11}. Hence, different weights are assigned to each tsunami and geodetic station (further details in Supplementary Information). In addition, due to the different behaviour of the cost functions for tsunami and geodetic data, we further assign different weights to both the entire data sets in order to avoid a possible unbalancing of the cost functions during the joint inversion.

The average slip model is calculated as a weighted mean of a subset of the explored models. This subset consists of the models with the lowest cost functions (0.5% of the total) and which fit satisfactorily the data. The weights are inversely related to the cost function, thus better models count more than the others. Dispersion of the model parameters around their average values is assessed by performing an a-posteriori analysis of the explored models ensemble^{10,14,16,32,71}, where the weighted standard deviation is taken as the error in the corresponding parameter. In this analysis the coefficient of variation (i.e. the standard deviation divided by the average slip value) is also computed for each subfault parameter (Fig. 3c).

- Chu, R. *et al.* Initiation of the great Mw 9.0 Tohoku-Oki earthquake. *Earth Planet. Sc. Lett.* **308**, 277–283, doi:10.1016/j.epsl.2011.06.031 (2011).
- Satake, K., Fujii, Y., Harada, T. & Namegaya, Y. Time and Space Distribution of Coseismic Slip of the 2011 Tohoku Earthquake as Inferred from Tsunami Waveform Data. *Bull. Seismol. Soc. Am.* **103**, 1473–1492, doi:10.1785/0120120122 (2013).
- Yamazaki, Y., Lay, T., Cheung, K. F., Yue, H. & Kanamori, H. Modeling near-field tsunami observations to improve finite-fault slip models for the 11 March 2011 Tohoku earthquake. *Geophys. Res. Lett.* **38**, L00G15, doi:10.1029/2011GL049130 (2011).
- Suzuki, W., Aoi, S., Sekiguchi, H. & Kunugi, T. Rupture process of the 2011 Tohoku-Oki mega-thrust earthquake (M9.0) inverted from strong-motion data. *Geophys. Res. Lett.* **38**, L00G16, doi:10.1029/2011GL049136 (2011).
- Pollitz, F. F., Bürgmann, R. & Banerjee, P. Geodetic slip model of the 2011 M9.0 Tohoku earthquake. *Geophys. Res. Lett.* **38**, L00G08, doi:10.1029/2011GL048632 (2011).
- Grilli, S. T. *et al.* Numerical Simulation of the 2011 Tohoku Tsunami Based on a New Transient FEM Co-seismic Source: Comparison to Far- and Near-Field Observations. *Pure Appl. Geophys.*, doi:10.1007/s00024-012-0528-y (2012).
- Iinuma, T. *et al.* Coseismic slip distribution of the 2011 off the Pacific Coast of Tohoku Earthquake (M9.0) refined by means of seafloor geodetic data. *J. Geophys. Res.* **117**, B07409, doi:10.1029/2012JB009186 (2012).
- Fujii, Y., Satake, K., Sakai, S., Shinohara, M. & Kanazawa, T. Tsunami source of the 2011 off the Pacific coast of Tohoku, Japan earthquake. *Earth Planets Space* **63**, 815–820, doi:10.5047/eps.2011.06.010 (2011).
- Yokota, Y. *et al.* Joint inversion of strong motion, teleseismic, geodetic, and tsunami datasets for the rupture process of the 2011 Tohoku earthquake. *Geophys. Res. Lett.* **38**, L00GL21, doi:10.1029/2011GL050098 (2011).
- Romano, F. *et al.* *Sci. Rep.* **2**, 385, doi:10.1038/srep00385 (2012).
- Hooper, A. *et al.* Importance of horizontal seafloor motion on tsunami height for the 2011 Mw9.0 Tohoku-Oki earthquake. *Earth Planet. Sc. Lett.* **361**, 469–479, doi:10.1016/j.epsl.2012.11.013 (2013).
- Maercklin, N., Festa, G., Colombelli, S. & Zollo, A. Twin ruptures grew to build up the giant 2011 Tohoku, Japan, earthquake. *Sci. Rep.* **2**, 709, doi:10.1038/srep00709 (2012).
- Yue, H. & Lay, T. Inversion of high-rate (1 sps) GPS data for rupture process of the 11 March 2011 Tohoku earthquake (Mw 9.1). *Geophys. Res. Lett.* **38**, L00G09, doi:10.1029/2011GL048700 (2011).
- Piatanesi, A. & Lorito, S. Rupture process of the 2004 Sumatra-Andaman earthquake from tsunami waveform inversion. *Bull. Seismol. Soc. Am.* **97**, S223–S231, doi:10.1785/0120050627 (2007).
- Lorito, S., Piatanesi, A., Cannelli, V., Romano, F. & Melini, D. Kinematics and source zone properties of the 2004 Sumatra-Andaman earthquake and tsunami: Nonlinear joint inversion of tide gauge, satellite altimetry, and GPS data. *J. Geophys. Res.* **115**, B02304, doi:10.1029/2008JB005974 (2010).
- Lorito, S. *et al.* Limited overlap between the seismic gap and the coseismic slip of the great 2010 Chile earthquake. *Nat. Geosci.* **4**, 173–177, doi:10.1038/NGEO1073 (2011).
- Zhao, D., Wang, Z., Umino, N. & Hasegawa, A. Mapping the mantle wedge and interpolate thrust zone of the northeast Japan arc. *Tectonophysics* **467**, 89–106, doi:10.1016/j.tecto.2008.12.017 (2009).
- Zhao, D., Huang, Z., Umino, N., Hasegawa, A. & Kanamori, H. Structural heterogeneity in the megathrust zone and mechanism of the 2011 Tohoku-Oki earthquake (Mw 9.0). *Geophys. Res. Lett.* **38**, L17308, doi:10.1029/cbGL048408 (2011).
- Zhao, D. Tomography and Dynamics of Western-Pacific Subduction Zones. *Monogr. Environ. Earth Planets* **1**, 1–70, doi:10.5047/meep.2012.00101.0001 (2012).
- Huang, Z. & Zhao, D. Relocating the 2011 Tohoku-oki earthquakes (M 6.0–9.0). *Tectonophysics* **586**, 35–45, doi:10.1016/j.tecto.2012.10.019 (2013).
- Kennett, B. L. N., Gorbato, A. & Kiser, E. Structural controls on the Mw 9.0 2011 Offshore-Tohoku earthquake. *Earth Planet. Sc. Lett.* **310**, 462–467, doi:10.1016/j.epsl.2011.08.039 (2011).
- Wang, K. & Kinoshita, M. Dangers of Being Thin and Weak. *Science* **342**, (2013); doi:10.1126/science.1246518 (2013).
- Chester, F. M. *et al.* Expedition 343 and 343T Scientists, 2013. Structure and Composition of the Plate-Boundary Slip Zone for the 2011 Tohoku-Oki Earthquake. *Science* **342**, doi:10.1126/science.1243719 (2013).
- Fulton, P. M. *et al.* Low Coseismic Friction on the Tohoku-Oki Fault Determined from Temperature Measurements. *Science* **342**, doi:10.1126/science.1243641 (2013).
- Ujiie, K. *et al.* Low Coseismic Shear Stress on the Tohoku-Oki Megathrust Determined from Laboratory Experiments. *Science* **342**, doi:10.1126/science.1243485 (2013).
- Strasser, M. *et al.* A slump in the trench: Tracking the impact of the 2011 Tohoku-Oki earthquake. *Geology* **41**, 935–938, doi: 10.1130/G34477.1 (2013).
- Faulkner, D. R., Mitchell, T. M., Behn, S., Hirose, T. & Shimamoto, T. Stuck in the mud? Earthquake nucleation and propagation through accretionary forearcs. *Geophys. Res. Lett.* **38**, L18303, doi:10.1029/2011GL048552 (2011).
- Mori, N., Takahashi, T., Yasuda, T. & Yanagisawa, H. Survey of 2011 Tohoku earthquake tsunami inundation and run-up. *Geophys. Res. Lett.* **38**, L00G14, doi:10.1029/2011GL049210 (2011).



29. Huang, Z., Zhao, D. & Wang, L. Seismic heterogeneity and anisotropy of the Honshu arc from the Japan Trench to the Japan Sea. *Geophys. J. Int.* **184**, 1428–1444, doi:10.1111/j.1365-246X.2011.04934.x (2011).
30. Tsuru, T. *et al.* Tectonic features of the Japan Trench convergent margin off Sanriku, northeastern Japan revealed by multi-channel seismic reflection data. *J. Geophys. Res.* **105**, 16403–16413 (2000).
31. Tsuru, T. *et al.* Along-arc structural variation of the plate boundary at the Japan Trench margin: Implication of interplate coupling. *J. Geophys. Res.* **107**, doi:10.1029/2001JB001664 (2002).
32. Cirella, A., Piatanesi, A., Tinti, E. & Cocco, M. Rupture process of the 2007 Niigata-ken Chuetsu-oki earthquake by non-linear joint inversion of strong motion and GPS data. *Geophys. Res. Lett.* **35**, L16306, doi:10.1029/2008GL034756 (2008).
33. Lorito, S., Romano, F., Piatanesi, A. & Boschi, E. Source process of the September 12, 2007, Mw 8.4, southern Sumatra earthquake from tsunami tide gauge record inversion. *Geophys. Res. Lett.* **35**, L02310, doi:10.1029/2007GL032661 (2008).
34. Rothman, D. Automatic estimation of large residual statics corrections. *Geophysics* **51**, 332–346, doi:10.1190/1.1442092 (1986).
35. Sen, M. & Stoffa, P. L. Nonlinear one-dimensional seismic waveform inversion using simulated annealing. *Geophysics* **56**, 1624–1638, doi:10.1190/1.1442973 (1991).
36. Sen, M. & Stoffa, P. L. *Global Optimization Methods in Geophysical Inversion* (Cambridge University Press, 2013).
37. Tanioka, Y. & Satake, K. Fault parameters of the 1896 Sanriku tsunami earthquake estimated from tsunami numerical modeling. *Geophys. Res. Lett.* **23**, 1549–1552 (1996).
38. Kumagai, H., Pulido, N., Fukuyama, E. & Aoi, S. High-frequency source radiation during the 2011 Tohoku-Oki earthquake, Japan, inferred from KiK-net strong-motion seismograms. *J. Geophys. Res.* **118**, 222–239, doi:10.1029/2012JB009670 (2013).
39. Yoshida, Y., Ueno, H., Muto, D. & Aoki, S. Source process of the 2011 off the Pacific coast of Tohoku Earthquake with the combination of teleseismic and strong motion data. *Earth Planets Space* **63**, 565–569, doi:10.5047/eps.2011.05.011 (2011).
40. Lay, T. & Kanamori, H. Insights from the great 2011 Japan earthquake. *Phys. Today* **64**, 33–39, doi:10.1063/PT.3.1361 (2011).
41. Ide, S., Baltay, A. & Beroza, G. C. Shallow Dynamic Overshoot and Energetic Deep Rupture in the 2011 Mw 9.0 Tohoku-Oki Earthquake. *Science* **332**, 1426–1429, doi:10.1126/science.1207020 (2011).
42. Tanioka, Y. & Satake, K. Tsunami generation by horizontal displacement of ocean bottom. *Geophys. Res. Lett.* **23**, 861–86 (1996).
43. Yagi, Y., Nakao, A. & Kasahara, A. Smooth and rapid slip near the Japan Trench during the 2011 Tohoku-Oki earthquake revealed by a hybrid back-projection method. *Earth Planets Space* **63**, 355–356, 94–101, doi:10.1016/j.epsl.2012.08.018 (2012).
44. Kubo, H. & Kakehi, Y. Source Process of the 2011 Tohoku Earthquake Estimated from the Joint Inversion of Teleseismic Body Waves and Geodetic Data Including Seafloor Observation Data: Source Model with Enhanced Reliability by Using Objectively Determined Inversion Settings. *Bull. Seismol. Soc. Am.* **103**, 1195–1220, doi:10.1785/0120120113 (2013).
45. Shao, G., Ji, C. & Zhao, D. Rupture process of the 9 March, 2011 Mw 7.4 Sanriku-Oki, Japan earthquake constrained by jointly inverting teleseismic waveforms, strong motion data and GPS observations. *Geophys. Res. Lett.* **38**, L00G20, doi:10.1029/2011GL049164 (2011).
46. Eberhart-Phillips, D. & Michael, A. J. Three-dimensional velocity structure, seismicity, and fault structure in the Parkfield Region, Central California. *J. Geophys. Res.* **98**, doi:10.1029/93JB01029, issn: 0148-0227 (1993).
47. Iinuma, T., Ohzono, M., Ohta, Y. & Miura, S. Coseismic slip distribution of the 2011 off the Pacific coast of Tohoku Earthquake (M 9.0) estimated based on GPS data—Was the asperity in Miyagi-oki ruptured? *Earth Planets Space* **63**, 643–648, doi:10.5047/eps.2011.06.013 (2011).
48. Loveless, J. P. & Meade, B. J. Geodetic imaging of plate motions, slip rates, and partitioning of deformation in Japan. *J. Geophys. Res.* **115**, B02410, doi:10.1029/2008JB006248 (2010).
49. Ruina, A. L. Slip instability and state variable friction laws. *J. Geophys. Res.* **88**, 10359–10370 (1983).
50. Rice, J. R. & Ruina, A. L. Stability of steady frictional slipping. *J. Appl. Mech.* **50**, 343–349 (1983).
51. Kaneko, Y., Avouac, J.-P. & Lapusta, N. Towards inferring earthquake patterns from geodetic observations of interseismic coupling. *Nat. Geosci.*, doi:10.1038/NGeo843 (2010).
52. Strasser, F. O., Arango, M. C. & Bommer, J. J. Scaling of the Source Dimensions of Interface and Intraslab Subduction-zone Earthquakes with Moment Magnitude. *Seismol. Res. Lett.* **81**, 941–950, doi:10.1785/gssrl.81.6.941 (2010).
53. Yamamoto, Y., Obana, K., Kodaira, S., Hino, R. & Shinohara, M. Structural heterogeneities around the megathrust zone of the 2011 Tohoku earthquake from tomographic inversion of onshore and offshore seismic observations. *J. Geophys. Res.* **119**, 1165–1180, doi:10.1002/2013JB010582 (2014).
54. Wang, Z., Huang, W., Zhao, D. & Pei, S. Mapping the Tohoku forearc: Implications for the mechanism of the 2011 East Japan earthquake (Mw 9.0). *Tectonophysics* **524–525**, 147–154, doi:10.1016/j.tecto.2011.12.032 (2012).
55. Yue, H. & Lay, T. Source Rupture Models for the Mw 9.0 2011 Tohoku Earthquake from Joint Inversions of High-Rate Geodetic and Seismic Data. *Bull. Seismol. Soc. Am.* **103**, 1242–1255, doi:10.1785/0120120119 (2013).
56. Noda, H. & Lapusta, N. Stable creeping fault segments can become destructive as a result of dynamic weakening. *Nature* **493**, doi:10.1038/nature11703 (2013).
57. Utsu, T. Aftershock activity of the 1896 Sanriku earthquake. *Zisin (J. Seism. Soc. Japan)* **2**(47), 89–92 (1994), in Japanese.
58. Kanamori, H. Mechanism of tsunami earthquakes. *Phys. Earth. Planet. Interiors* **6**, 346–359 (1972).
59. Okal, E. 2012. From 3-Hz P waves to 0S2: No evidence of a slow component to the source of the 2011 Tohoku earthquake. *Pure Appl. Geophys.* **170**, 863–973, doi:10.1007/s00024-012-0500-X (2013).
60. McGuire, J. J. & Jordan, T. H. Further evidence for the compound nature of slow earthquakes: The Prince Edward Island earthquake of April 28, 1997. *J. Geophys. Res.* **105**, 7819–7827 (2000).
61. Sato, M. *et al.* Displacement Above the Hypocenter of the 2011 Tohoku-Oki Earthquake. *Science* **332**, doi:10.1126/science.1207401 (2011).
62. Ito, Y. *et al.* Frontal wedge deformation near the source region of the 2011 Tohoku-Oki earthquake. *Geophys. Res. Lett.* **38**, L00G05, doi:10.1029/2011GL048355 (2011).
63. Kido, M., Osada, Y., Fujimoto, H., Hino, R. & Ito, Y. Trench-normal variation in observed seafloor displacements associated with the 2011 Tohoku-Oki earthquake. *Geophys. Res. Lett.* **38**, L24303, doi:10.1029/2011GL050057 (2011).
64. Hayes, G. P., Wald, D. J. & Johnson, R. Slab1.0: A three-dimensional model of global subduction zone geometries. *J. Geophys. Res.* **117**, B01302, doi:10.1029/2011JB008524 (2012).
65. Miura, S. *et al.* Structural characteristics off Miyagi forearc region, the Japan Trench seismogenic zone, deduced from a wide-angle reflection and refraction study. *Tectonophysics* **407**, 165–188, doi:10.1016/j.tecto.2005.08.001 (2005).
66. Bellahsen, N., Faccenna, C. & Funicello, F. Dynamics of subduction and plate motion in laboratory experiments: Insights into the “plate tectonics” behavior of the Earth. *J. Geophys. Res.* **110**, B01401, doi:10.1029/2004JB002999 (2005).
67. Trasatti, E., Kyriakopoulos, C. & Chini, M. Finite element inversion of DInSAR data from the Mw 6.3 L'Aquila earthquake, 2009 (Italy). *Geophys. Res. Lett.* **38**, doi:10.1029/2011GL046714 (2011).
68. Abaqus, Version 6.9, Dassault Systèmes Simulia Corp. Providence, www.simulia.com (Date of access: 11/06/2014) (2011).
69. Yamazaki, Y., Kowalik, Z. & Cheung, K. F. Depth-integrated, non-hydrostatic model for wave breaking. *Int. J. Numer. Meth. Fluids* **61**, 473–497, doi:10.1002/fld.1952 (2009).
70. Yamazaki, Y., Cheung, K. F. & Kowalik, Z. Depth-integrated, non-hydrostatic model with grid nesting for tsunami generation, propagation, and run-up. *Int. J. Numer. Meth. Fluids* **67**, 2081–2107, doi:10.1002/fld.2485 (2011).
71. Romano, F., Piatanesi, A., Lorito, S. & Hirata, K. Slip distribution of the 2003 Tokachi-oki Mw 8.1 earthquake from joint inversion of tsunami waveforms and geodetic data. *J. Geophys. Res.* **115**, B11313, doi:10.1029/2009JB006665 (2010).
72. Spudich, P. & Miller, D. P. Seismic site effects and the spatial interpolation of earthquake seismograms: results using aftershocks of the 1986 North Palm Springs, California, earthquake. *Bull. Seismol. Soc. Am.* **80**, 1504–1532 (1990).

Acknowledgments

We acknowledge Fabio Corbi, Gaetano Festa, Francesco Pio Lucente, and Elena Spagnuolo for the fruitful discussions. We warmly acknowledge the availability of Patrick Fulton to discuss about sensitivity of friction values to slip values. We wish to thank all of the data providers who made this study possible, and in particular JMA (stations Boso and Tokai), NOWPHAS (coastal wave gauges and GPS-buoys), JAMSTEC (stations KPGs and MPGs), ERI at the University of Tokyo (stations TM1, TM2, P02, and P06), NOAA (DART 21413, 21418, 21419), RFRHR (DART 21401), and GEONET (GPS data). Some Figures were drawn with Generic Mapping Tools (<http://gmt.soest.hawaii.edu/>, Date of access: 11/06/2011). This work has been partially funded by EC project ASTARTE - Assessment, Strategy And Risk Reduction for Tsunamis in Europe. Grant 603839, 7th FP (ENV.2013.6.4-3 ENV.2013.6.4-3).

Author contributions

F.R., E.T. and S.L. were involved in all of the phases of this study. C.P. contributed to the interpretation and discussion of results, and to paper writing. A.P. contributed to design the experiment and to discuss and interpret the results. Y.I. and K.H. provided part of the geodetic and tsunami data sets, and contributed to results interpretation. D.Z. provided the seismic tomographic model and contributed to the discussion of results. P.L. provided support for the computationally expansive numerical tsunami modelling. M.C. promoted the experiment, contributed to results interpretation and paper writing. All authors reviewed the final manuscript.

Additional information

Supplementary information accompanies this paper at <http://www.nature.com/scientificreports>

Competing financial interests: The authors declare no competing financial interests.



How to cite this article: Romano, F. *et al.* Structural control on the Tohoku earthquake rupture process investigated by 3D FEM, tsunami and geodetic data. *Sci. Rep.* **4**, 5631; DOI:10.1038/srep05631 (2014).



This work is licensed under a Creative Commons Attribution-NonCommercial-ShareAlike 4.0 International License. The images or other third party material in this

article are included in the article's Creative Commons license, unless indicated otherwise in the credit line; if the material is not included under the Creative Commons license, users will need to obtain permission from the license holder in order to reproduce the material. To view a copy of this license, visit <http://creativecommons.org/licenses/by-nc-sa/4.0/>